Development of a 7.2-, 8.4-, and 32-Gigahertz (X-/X-/Ka-Band) Three-Frequency Feed for the Deep Space Network

P. H. Stanton,[1] D. J. Hoppe,[1] and H. Reilly[1]

This article summarizes the design of a three-frequency feed for the Deep Space Network supporting the 32-GHz downlink, 8.4-GHz downlink, and 7.2-GHz uplink bands simultaneously. Monopulse tracking is also provided at 32 GHz. The design combines high-power uplink operation and ultra-low-noise receive capability in a single feed with no need for frequency-selective surfaces or external diplexers. The key components of the feed will be described along with special considerations taken into account during their design. Experimental results, lessons learned, and ideas for future improvement are also included.

I. Introduction

The Telecommunications and Mission Operations Directorate (TMOD) road map, described in [1], highlights the need to implement a 32-GHz (Ka-band) receive capability in the Deep Space Network in order to provide the increased data capacity required for future deep-space missions. In addition, the majority of existing missions as well as those in the near-term plan will continue to employ 8.4-GHz (X-band) downlink and 7.2-GHz (X-band) uplink. This implies that present X-band performance must be maintained along with the addition of Ka-band.

One option for adding the Ka-band capability in a beam-waveguide (BWG) environment is to use frequency-selective surfaces (FSS) to separate the X-band and Ka-band signals [2]. This approach has the advantage that relatively simple X- and Ka-band feeds are required. Isolation between the two bands is easy to achieve due to the large spatial separation. Disadvantages include the real estate required, the need for separate dewars for the X-band and Ka-band low-noise amplifiers (LNAs), and the noise added due to scattering from the FSS used to diplex the signals.

This article describes a second approach, development of a single feed that accommodates all of the required frequencies in one package. The package is compact and has low noise relative to diplexing with an FSS. With a redesign of the flared portion, the three-frequency feed is also compatible with conventional (non-beam-waveguide) antennas. A single, but larger, dewar is required to house all of the LNAs. An additional complexity is that the phase center of the horn at X-band is not coincident with the phase

[1] Communications Ground Systems Section.

The research described in this publication was carried out by the Jet Propulsion Laboratory, California Institute of Technology, under a contract with the National Aeronautics and Space Administration.

center at Ka-band. The feed is necessarily complicated and requires careful design in order to achieve low-noise performance, achieving both low-loss diplexing and high-power operation. These design issues and the resulting performance are the subject of this article. Low-noise amplifier and cryogenic design for the feed, noise-temperature measurements, and feed performance on the antenna will be subjects of future articles.

II. Requirements

The key requirements for the feed system are summarized below.

(1) Frequencies of operation
   (a) X-band receive 8.400–8.585 GHz
   (b) X-band transmit 7.145–7.190 GHz
   (c) Ka-band receive 31.8–32.3 GHz

(2) Polarization
   (a) Ka-band monopulse right-hand circular polarization
   (b) All others dual circular

(3) Horn gain/patterns compatible with 34-m BWG antennas, e.g., DSS 26

(4) Noise temperature, Te, feed plus LNA
   (a) X-band 9.3 K, +1.2 K, −1.0 K
   (b) Ka-band sum 16.6 K, +3.0 K, −3.0 K
   (c) Ka-band error 21.6 K, +5.0 K, −4.0 K

(5) Return loss
   (a) 8.4–8.45 GHz, 30.0 dB
   (b) 8.45–8.50 GHz, 26.0 dB
   (c) 8.585 GHz, 22.0 dB
   (d) 31.8–32.3 GHz, 30.0 dB
   (e) 7.145–7.190 GHz, 24.0 dB

(6) X-band transmit/receive isolation
   (a) 7.145 GHz, 52.0 dB
   (b) 7.190 GHz, 52.0 dB

(7) Transmitter power handling, 20 kW continuous wave

A mechanical requirement for the horn design is that the X-/X-/Ka-band common aperture must fit into the existing X-band feed position of the DSN 34-m BWG antenna with less than 0.1 percent loss due to feed blockage. The high-level requirement is that the gain-to-noise temperature (G/T) loss of the BWG antenna with the X-/X-/Ka-band feed as compared with the optimum single-band horn must be less than 0.1 dB for X-band and 0.2 dB for Ka-band.

III. Overall Configuration

Figure 1 shows a photograph of the X-/X-/Ka-band horn with monopulse coupler and linear polarization combiners attached to the X-band ports. The basic internal configuration of the X-/X-/Ka-band horn is shown in Fig. 2.

The horn is fed at Ka-band through a monopulse coupler, similar in design to that described in [3]. The sum mode at Ka-band, a circularly polarized TE_{11} mode, is excited using a commercial ortho-mode junction and polarizer. It passes through the center of the monopulse coupler and enters the horn as shown at the left-hand side of Fig. 2. The difference mode, a circularly polarized TE_{21} mode, is excited through the monopulse coupler arms and enters the horn as well. These modes are transformed to the hybrid HE_{11} and HE_{21} modes in the Ka-band mode-converter section. The X-band downlink signal is extracted in the X-band downlink junction, which consists of four waveguides that exit the circular guide radially at 90-deg intervals. These waveguides excite a pair of orthogonal TE_{11} modes in the horn. A straight corrugated section and slight flare follow. The X-band uplink signal is injected in the X-band uplink junction, which is similar in design to the downlink junction. Next the TE_{11} modes at X-band are transformed into the HE_{11} mode in the X-band mode-converter section. Finally, the horn is flared at a constant angle with a constant groove profile to the final aperture size. The following sections will describe the various horn components in greater detail.

IV. Monopulse Tracking Coupler

As discussed above, connected to the 10.9474-mm-diameter end of this horn is a monopulse tracking coupler as shown in Fig. 1. This coupler has both a sum port (TE_{11} mode) and a difference port (TE_{21} mode). As described in [3], the TE_{21} mode is excited by means of eight symmetrically placed Ka-band side-wall couplers mounted on the central waveguide. These are in turn connected through a series of combiners to generate circular polarization. When radiated by the corrugated horn, the TE_{21} mode has

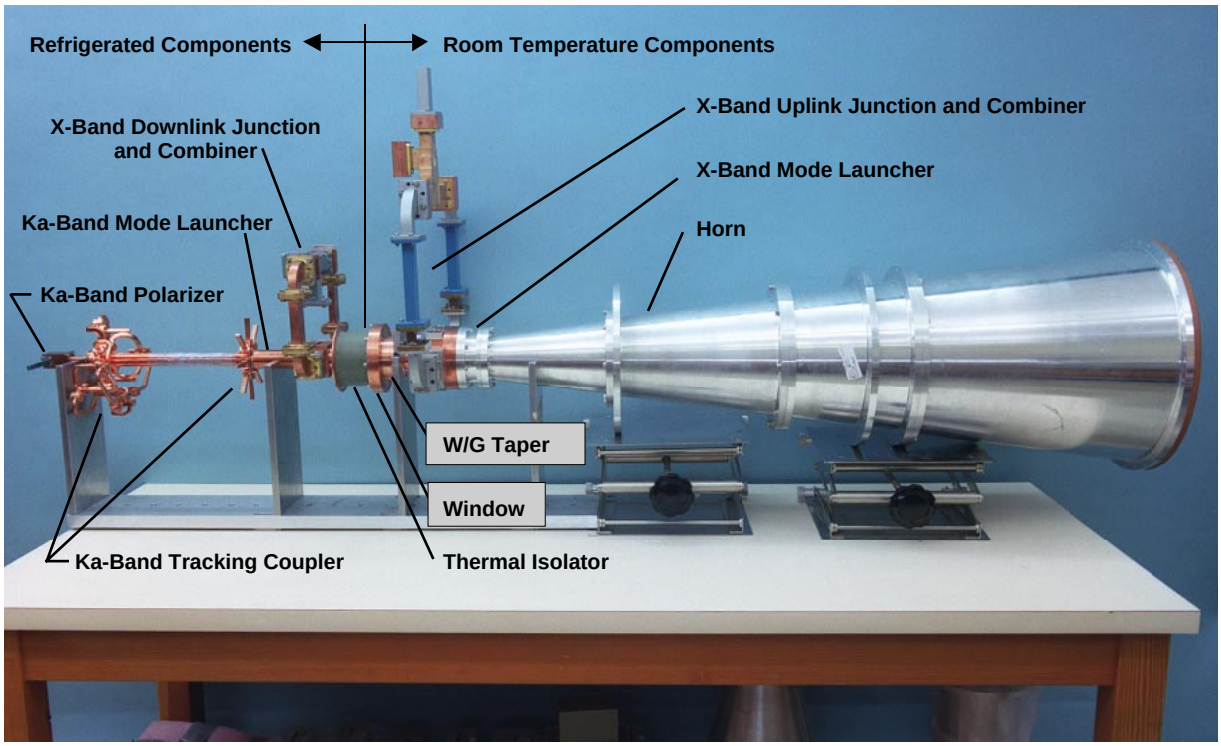

Fig. 1. The X-/X-/Ka-band horn with monopulse coupler.

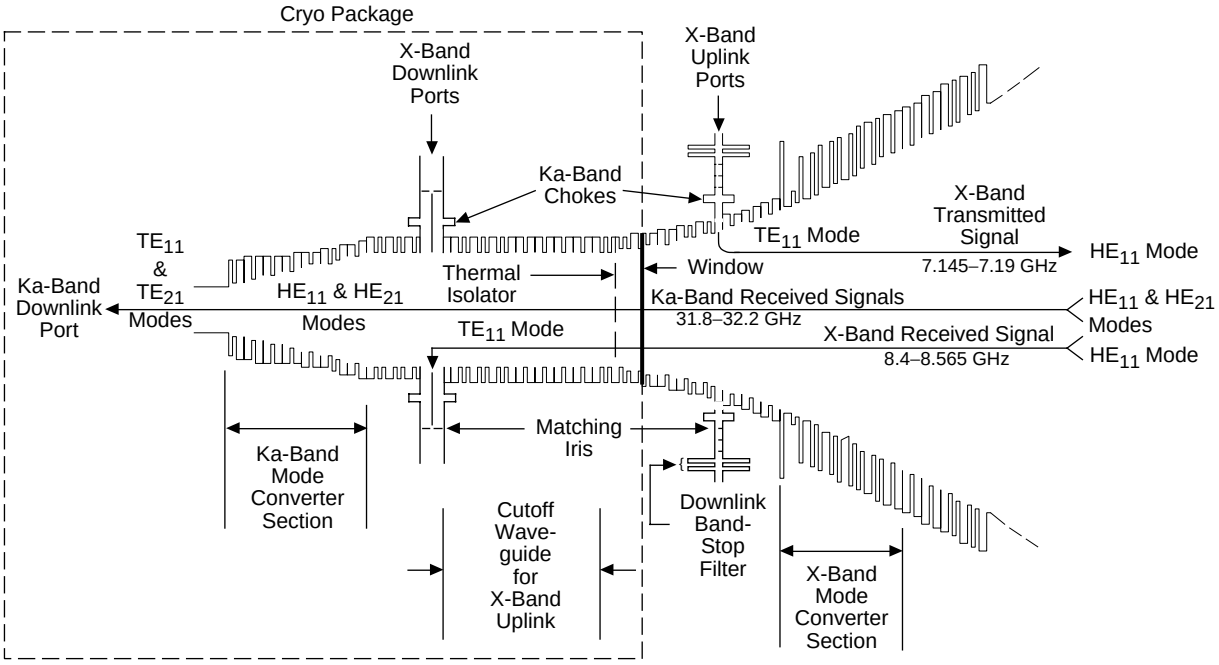

Fig. 2. The X-/X-/Ka-band horn internal geometry.

a theoretical null on axis. The magnitude of the power received in the TE_{21} mode relative to the TE_{11} mode (sum beam) is proportional to the θ pointing error (angle relative to the antenna boresite). The azimuthal error, ϕ, is proportional to the phase difference between the sum and difference signals. Thus, by measuring the complex ratio of the sum and difference signals, pointing updates can be generated that will drive the difference signal and consequently the antenna pointing error to zero. Measurements made of the overall assembled horn at these ports show a return loss of greater than 25 dB (see Figs. 3 and 4). Although these values are not technically within the specification, the only effect is on the feed noise temperature at Ka-band. Calculations indicate that a 25-dB feed return loss will have a minor effect on the noise temperature, adding an additional 0.34 K to the overall temperature.

V. Ka-Band Mode Converter

The Ka-band mode converter transforms the TE_{11} and TE_{21} modes launched by the monopulse coupler into HE_{11} and HE_{21} modes. The zero-impedance smooth-wall circular waveguide is transformed into a high-impedance corrugated waveguide using a series of grooves that taper in width as well as depth. The grooves begin with a depth of 4.9022 mm, near one-half wavelength, and finish at 2.54 mm, the nominal groove depth for the Ka-band portion of the horn. The final groove width is 2.8956 mm, and the lands are 1.016 mm. This shallow corrugation supports the Ka-band HE_{11} and HE_{21} modes out to the X-band mode converter. Finally, the Ka-band mode converter tapers up to a waveguide diameter large enough to support the X-band downlink TE_{11} mode, a 22.352-mm-diameter inner dimension with 2.54-mm-deep grooves. The design of the Ka-band mode converter was optimized by hand using mode-matching software [4], considering both the TE_{11} mode and TE_{21} mode return losses simultaneously.

VI. X-Band Downlink Junction

The next component in the feed is the X-band downlink junction. A pair of rectangular waveguides 180 deg apart are required to excite the TE_{11} mode and avoid generating undesired modes. A second pair of waveguides 90 deg from the above is required to generate circular polarization. The rectangular

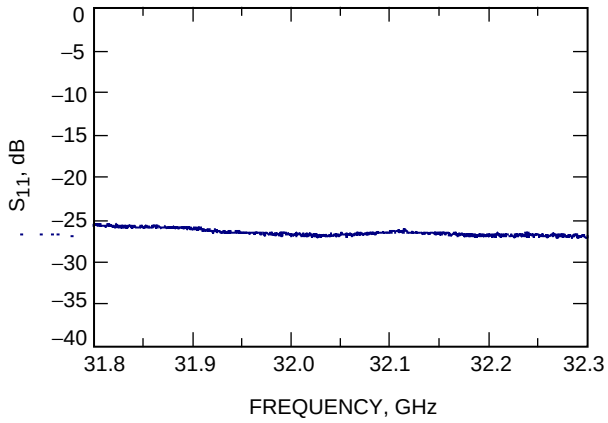

Fig. 3. Ka-band sum port match.

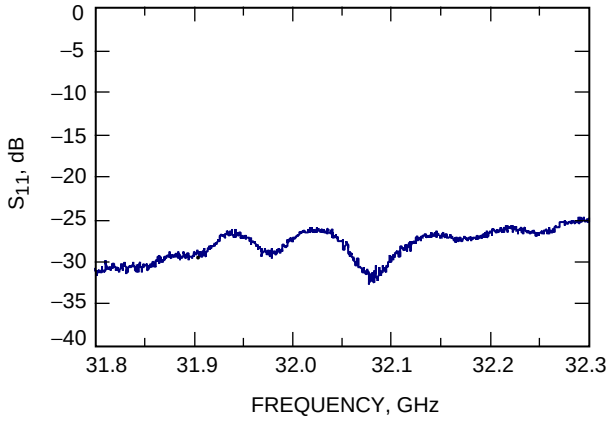

Fig. 4. Ka-band difference port match.

waveguide height feeding the junction is reduced from the standard WR112 height of 12.6238 mm to the width of two grooves and a land, 6.8072 mm (see Fig. 2). Entering two grooves simultaneously provides for a wideband match relative to entering only a single groove. The junction has a pair of circular chokes, which keep the Ka-band confined inside the corrugated circular waveguide. The chokes are placed to present a short circuit at what would be the bottom of the groove, making the corrugations inside the horn appear continuous at Ka-band.

The distance between the Ka-band mode converter, which acts as a short at the X-band downlink frequency band, and the X-band downlink junction is adjusted to optimize the match of these X-band ports. This optimized distance results in a raw return loss of approximately 4.5 dB across the downlink band. Careful measurements of this return loss were taken using the approach described in the Appendix. These measured data were used as a termination in a mode-matching model of the iris-loaded input arm. The size and position of the iris were optimized automatically to give the best return loss possible across the downlink band. It was found that the rectangular waveguide arms could be matched within the specification using a single inductive iris.

With two rectangular ports combined for linear polarization, as shown in Fig. 1, the X-band downlink junction has a return loss of better than 26 dB from 8.4 to 8.5 GHz (Fig. 5). Once again the 26-dB return loss does not meet the 30-dB requirement. In this case, calculations predict a negligible 0.1-K increase in noise temperature due to the excessive return loss. This downlink port is isolated from the uplink port by approximately 77 dB or greater in the uplink band of 7.145 to 7.190 GHz (Fig. 6). This isolation

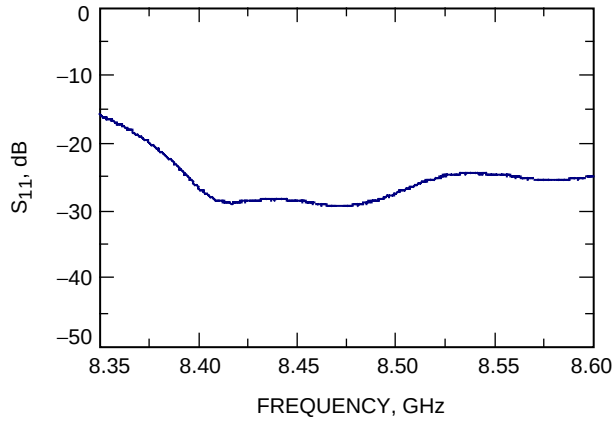

Fig. 5. X-band receive match.

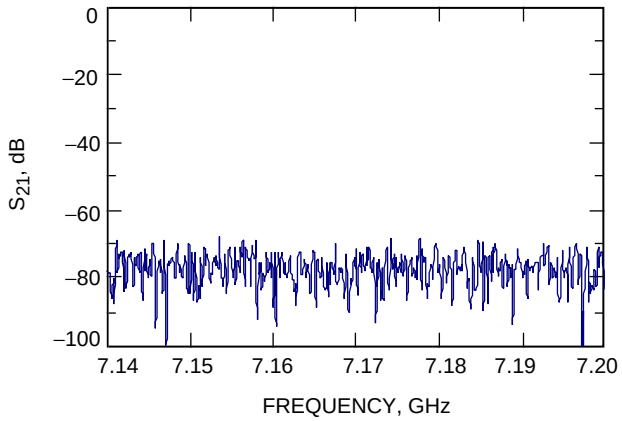

Fig. 6. X-band transmit-to-receive isolation.

is obtained because the corrugated waveguide between these two ports is generally below cutoff at the uplink frequency band. Further isolation is provided within the LNA itself.

VII. Thermal Gap and Window Assembly

The next part of the horn is a straight section of corrugated waveguide that is at cutoff for the X-band uplink frequency but will support the downlink frequency. This section acts as a filter to keep nearly all of the multi-kilowatt uplink power out of the X-band downlink ports. The horn, up to this point, is in a cryogenic package. The thermal gap at the top of the dewar comes next with its X- and Ka-band chokes. Beyond this cryogenic package is a 0.0127-mm-thick kapton vacuum window that also includes X- and Ka-band chokes to prevent signal leakage. Following this window, the waveguide tapers up to a size large enough to support the uplink TE_{11} mode.

Although the overall length of the cutoff corrugated waveguide section is fixed by the required isolation between X-band transmit and receive ports, the distribution of that waveguide between the cryogenic and ambient temperature environments is a key free parameter in the design. Noise performance is optimum if the cutoff section is housed totally within the cryogenic environment. Noise contributions from this section at the X-band receive frequency are approximately 0.2244 K/cm when the section is at ambient temperature and near 0.004 K/cm when it is at a cryogenic temperature of 8 K. On the other hand, as the vacuum window moves closer to the transmit ports, more transmit power decays into the kapton window

and cooled waveguide. This generates heat that must be removed from the system by the refrigerator. The RF power can also damage the kapton window. These effects were analyzed in order to ensure a safety margin for the design of the horn. A discussion of the analysis technique and results follows.

A perturbation technique was used to compute the approximate power dissipated in the waveguide walls and window when the transmit power is injected into the horn. A mode-matching model of the horn from the transmit junction back toward the Ka-band input was used. The transmitter power was injected into the horn, and the total fields were computed everywhere, assuming no loss. Both propagating and evanescent modes were included. The wall surface currents were then computed, and the finite conductivity of the walls was used to compute the approximate power lost in the waveguide. For the kapton window and any thermal backing material, the total field inside the volume of the window was used along with the complex dielectric constant of the materials to compute the power lost inside the window.

For the present calculations, 20 kW of transmitter power was injected back toward the Ka-band input. This provides approximately a 3-dB margin in the calculation since in reality half of the power injected in the transmit junction will travel directly forward and only half will travel backward and be reflected by the cutoff waveguide section. Theoretical copper loss was assumed in the calculation. In practice, higher losses are expected, using up a portion of the 3-dB margin discussed above.

Figure 7 shows the power dissipated per section. Section 1 corresponds to the input junction, section 44 to the window, and section 68 to the thermal gap. The fields are propagating up to approximately section 20, where the cutoff waveguide begins. After this point, an exponential decay of the dissipated power per section is seen, 4.528 dB/cm. Figure 8 shows the integrated power versus section number, indicating that a total power of 86.5 W is dissipated, the vast majority of which is outside the cryogenic vessel. Figure 9 shows the residual power versus section number, and indicates that approximately 1.70 mW of power must be handled by the cryogenic system after the thermal gap. This is considered to be well within the capability of the present design, and the associated loss of refrigerator capacity should contribute a negligible increase in system noise temperature. Figure 10 shows the dissipated power in the kapton window and losses in adjacent sections, assuming they were filled with low-loss foam. For these cases, the dielectric constant for kapton was assumed to be 3.7 with a loss tangent of 0.0027, and that

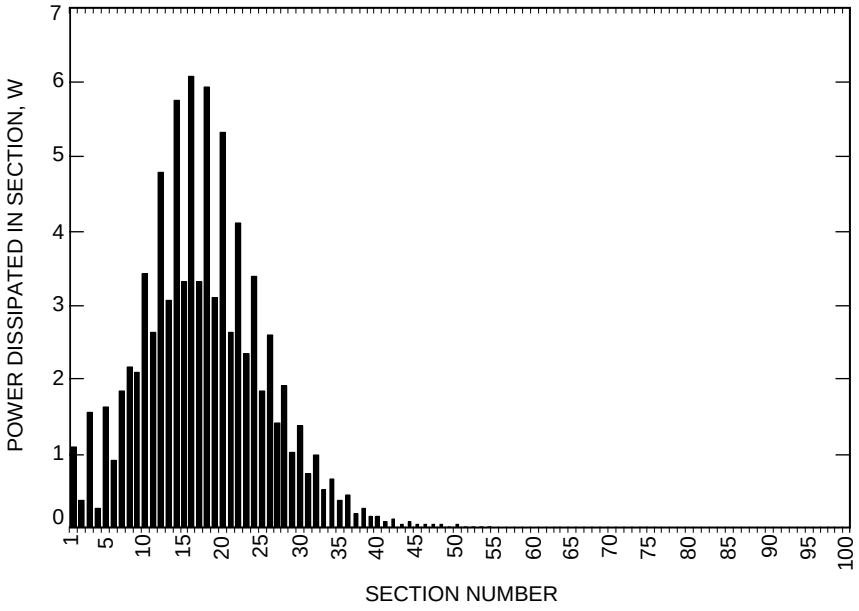

Fig. 7. Dissipation per waveguide section.

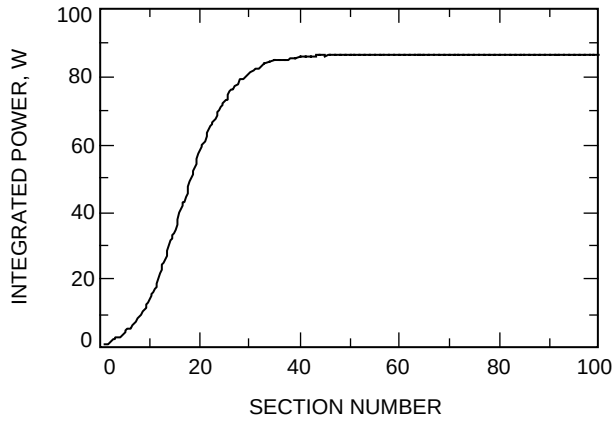

Fig. 8. Integrated dissipation versus horn position.

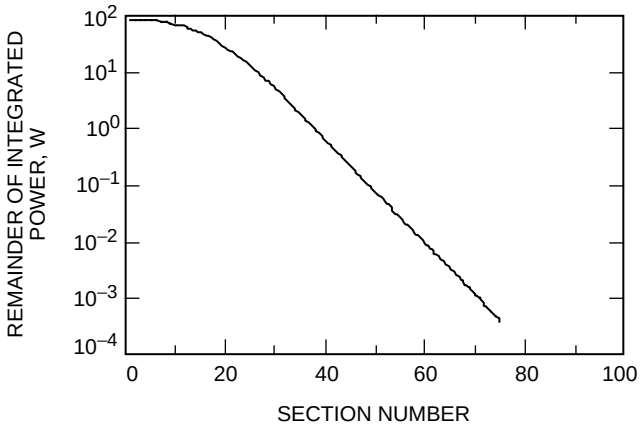

Fig. 9. Residual dissipation versus horn position.

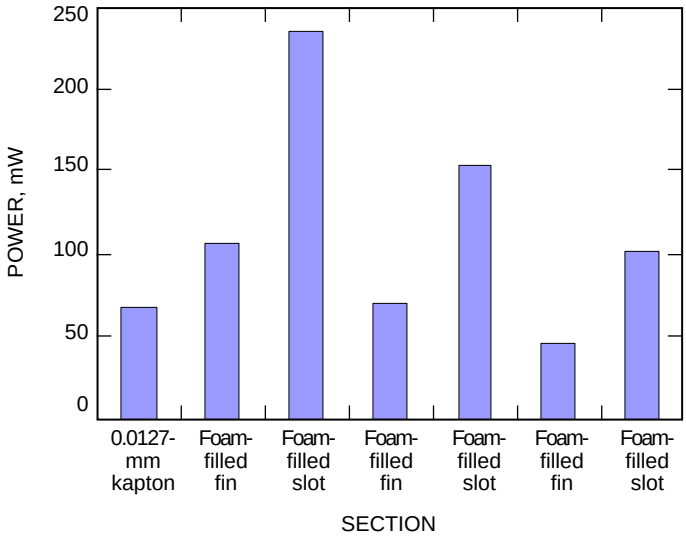

Fig. 10. Window dissipation.

of the foam to be 1.04 with a loss tangent of 0.0003. The computed power in the window, 67 mW, is considered to be within design limits. The present design does not employ any dielectric foam backing for the window. Although the prototype horn withstood full-power testing, a future iteration of the design should investigate improvements in the window configuration.

VIII. X-band Uplink Junction

As with the downlink junction, the X-band uplink junction consists of four rectangular waveguides intersecting the horn as shown in Fig. 1. The heights of these waveguides are reduced to the width of a single corrugation groove, 2.8956 mm. This is done to have minimum impact on the periodic structure inside the horn, thus avoiding unwanted mode conversion or mismatch to the other signals traveling through this section of the horn. This junction has a pair of circular chokes that keep the Ka-band confined to the inside of the horn. These chokes are placed at a radius, which presents a reflection of the Ka-band signal equivalent to the short at the bottom of other grooves. Again, this is to prevent unwanted mode conversion.

Each of the four rectangular waveguides is matched to the circular horn by a series of irises. As with the downlink junction, the matching structures were optimized automatically using the mode-matching method and actual measurements of the raw reflection coefficient of the junction. In this case, match in the uplink frequency band and the effective short position in the receive band were considered in the optimization process. Three irises were required to provide the appropriate matching and short position over the bandwidth.

An auxiliary stop-band filter at the downlink frequency is also included in each of these rectangular waveguides to further isolate the transmit waveguide from the horn over the downlink band. This filter is made up of two grooves in the reduced-height, 2.8956-mm, WR137 waveguide used in the junction. The grooves are in the broad wall of the waveguide. Each groove is 8.9662-mm deep and 2.9464-mm long, with a separation of 2.1082 mm between the two grooves. The distance this matching device/stop-band filter is placed from the waveguide junction is chosen to minimize the mismatch effect on the downlink signal.

With two rectangular ports combined for linear polarization, as shown in Fig. 1, the X-band uplink junction has a return loss of better than 27 dB from 7.145 to 7.190 GHz (Fig. 11). This junction, including the X-band downlink stop-band filter, provides isolation of 55 dB or greater over a frequency band of 8.4 to 8.5 GHz, as shown in Fig. 12. An isolation level of 55 dB corresponds to a negligible noise contribution from the ambient transmitter ports, approximately 0.950 mK.

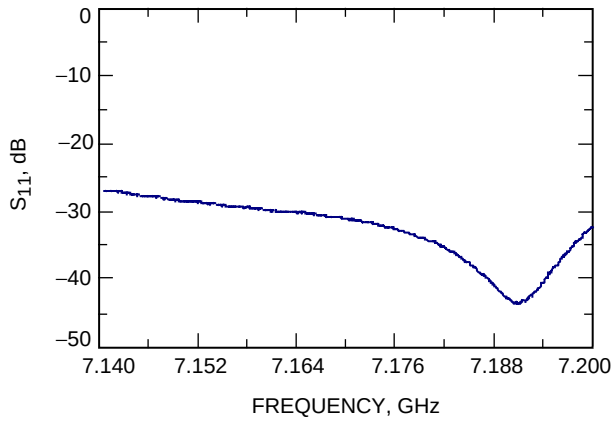

Fig. 11. X-band transmitter match.

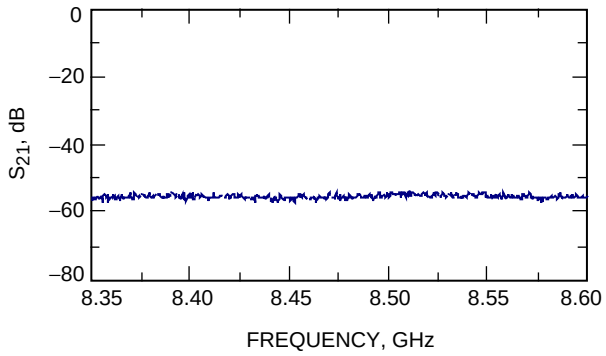

Fig. 12. X-band receive-to-transmit isolation.

IX. X-Band Diplexer

To further limit the amount of transmitter beam noise that gets to the X-band receiver, an existing diplexer is inserted between the transmitter and the feed. This diplexer provides a stop-band filter in the frequency range of 8.2 to 8.6 GHz. The loaded receive port of this diplexer absorbs any noise that is trapped between this stop-band filter and the ones that are built into the feed's X-band uplink junction, thus preventing high Q resonances.

X. X-Band Mode Converter

Near the throat of the horn there is a transition from the shallow grooves, 2.54 mm, which support only the Ka-band HE_{11} and HE_{21} modes, to deeper grooves, 11.684 mm, which support the HE_{11} mode at X-band and the HE_{11} and HE_{21} modes at Ka-band. This transition is accomplished via the X-band mode converter (HE_{11}–TE_{11} or TE_{11}–HE_{11}). The design of this mode converter presented one of the most difficult challenges in the design of the horn.

This X-band mode converter must, in addition to accomplishing the X-band mode conversion, present a low mismatch to the X- and Ka-band signal and maintain the Ka-band HE_{11} and HE_{21} modes across it. Initially the mode converter was designed as a series of dual-depth grooves, but this configuration included a number of narrow deep grooves, which later proved to be quite lossy and, therefore, a large contributor to the feed noise temperature. A new X-band mode converter was designed with a single deep matching groove to improve the loss. Details regarding the evolution of this important horn component are given in the next few paragraphs.

Figures 13 through 15 summarize a series of calculations that was carried out to determine the relative noise contribution from each of the X-band mode converters considered in the design. It should be noted that these calculations were completed after the second generation of the feed was measured, indicating an unexpectedly high noise-temperature contribution.

In all three simulations, the horn was fed conventionally through a transition section that converted from a smooth-walled circular waveguide into the shallow-grooved (Ka-band) corrugated waveguide. This was followed by the X-band mode converter and the flared portion of the horn. Copper walls at a physical temperature of 300 K were assumed, and the noise-temperature contribution from each section was computed using the technique described in Section VII. These assumptions will give lower bounds on the loss and noise temperature. True loss and temperature depend on the surface roughness and true resistivity of the copper employed. All calculations were carried out at 8.425 GHz.

In the initial version of the horn, the first generation, seven dual-depth grooves made up the mode converter [5]. These grooves were split with one portion's depth corresponding to the Ka-band groove and

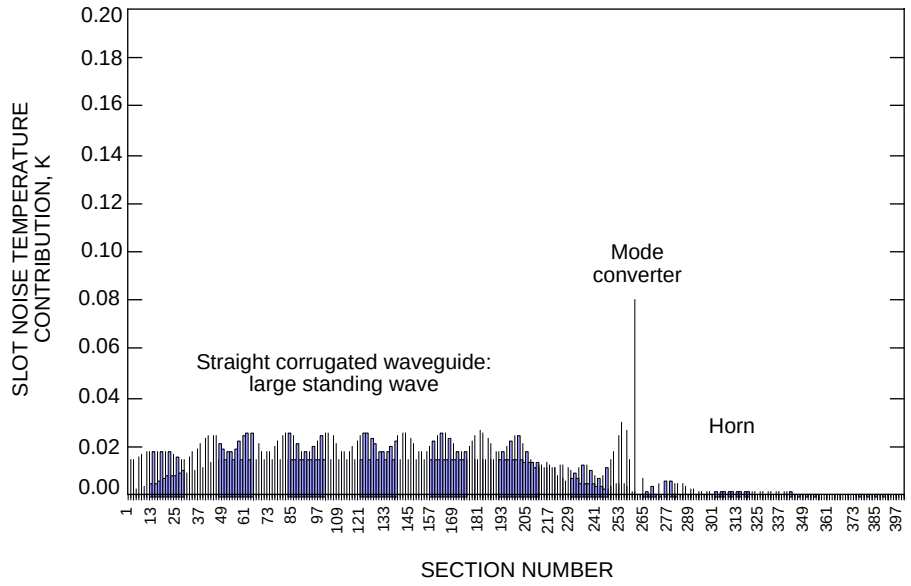

Fig. 13. The first-generation X-band mode converter.

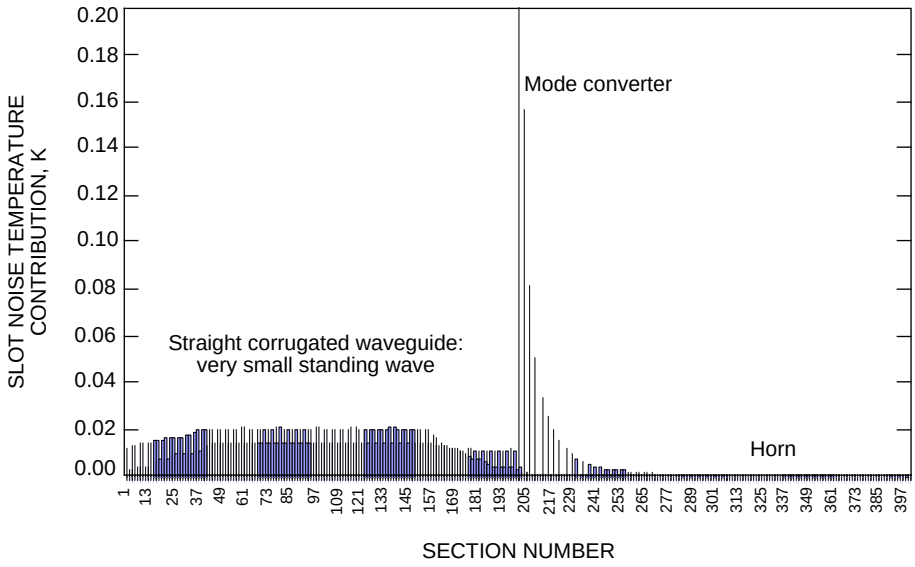

Fig. 14. The second-generation X-band mode converter.

the other portion's depth corresponding to the X-band groove. Gradually a greater and greater percentage of the overall groove is dedicated to the X-band depth as one moves along the converter. This provides a smooth transition between the two corrugated sections. The noise temperature contribution per section for this mode converter is plotted in Fig. 13. A standing wave pattern is apparent in the straight corrugated waveguide. This is due to a multimode reflected wave from the X-band mode converter that is trapped between it and the Ka-band input transition section. The existence of this small reflection was known from time-domain measurements of the feed reflection. When the noise-temperature contribution of a feed using this mode converter was measured, it was higher than expected. At the time it was incorrectly assumed that the excess noise temperature was related to the reflected wave, and the mode-converter match was improved in the second-generation feed. In fact, the true source of the excess noise is visible in Fig. 13. The first dual-depth groove in the mode converter, section 260, is extremely lossy. It contains

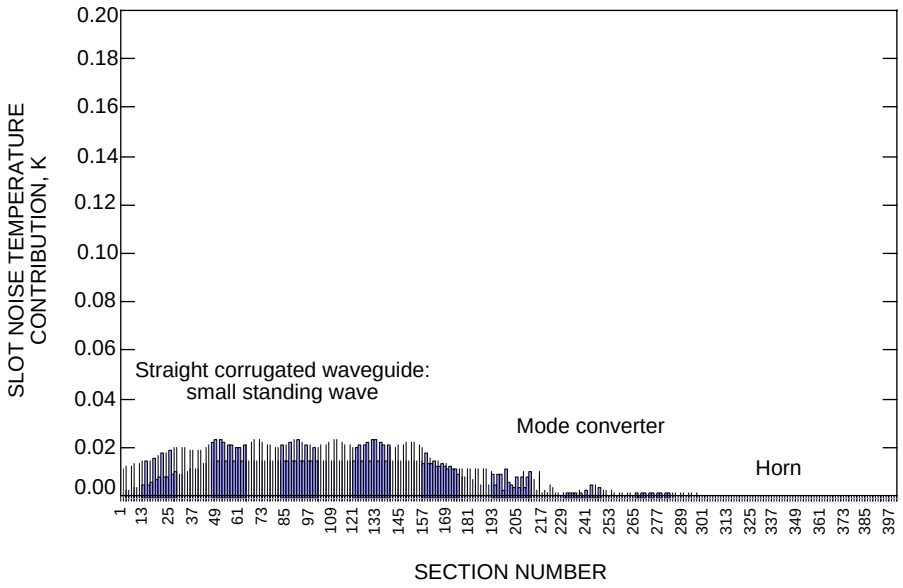

Fig. 15. The third-generation X-band mode converter.

a very deep (X-band depth), narrow (1.3462-mm) groove section. Unfortunately, these calculations were not available at the time the mode converter was redesigned for the second-generation feed.

In order to improve the converter mismatch in the second-generation of the horn, 15 dual-depth grooves were used in the mode converter. This resulted in a better match, as indicated in Fig. 14. Unfortunately, this match is achieved by including many more dual-depth grooves with narrow, deep segments. In this case, the initial groove has a very narrow (0.19304-mm) portion dedicated to X-band depth. This slot, near section 200, is extremely lossy, as indicated in the figure. A large number of the subsequent slots are also very lossy. Measurements of this feed did indicate a significantly higher noise temperature than that of the first-generation feed. Efforts to diagnose the problem with this version of the feed led to the development of the computational tools described here and in Section VII.

As a result of the above calculations, a third-generation mode converter was designed with the goal of achieving the best possible match and patterns without the use of deep, narrow slots. It was found that a single deep slot, approximately 15.24 mm in depth, appropriately spaced could match the two different-depth groove sections at X-band and have minimal effect on the Ka-band sum patterns. This is a narrow band but acceptable solution. Results for this case are shown in Fig. 15. A small standing wave is present but, since no narrow, deep grooves are present, the mode converter's contribution to the feed noise temperature is insignificant. The effect of the single slot on the Ka-band difference patterns was not considered in the design. Some degradation of these patterns was found and is discussed in the next section.

XI. Horn Flare Section

The horn taper angle and aperture sizes were optimized for the operational DSN 34-m BWG antennas. The zeroth-order Gaussian iteration technique was employed to design the horn's parameters in conjunction with the existing parameters of the DSN 34-m BWG antenna [6]. The physical optics program was then used to calculate BWG antenna gain and noise temperature with various cases of the horn design. The design iteration was continued until the design requirements were met.

The final design parameters of the horn include an aperture inside diameter of 391.16 mm and a horn taper angle of 8.10 deg. The gain of the horn at X-band (8.425 GHz) is 27.9 dBi; for Ka-band (32.05 GHz)

it is 29.4 dBi. It is also important to note that there is a 596.9-mm separation between X-band and Ka-band phase centers where the phase center is about 723.9 mm below the horn aperture at X-band and 1.3208 m for Ka-band.

Figure 16 shows the measured and computed sum patterns for the horn at 32.3 GHz. Since the full aperture of the horn exceeds the near-field range's scan capability at 32.3 GHz, a reduced-aperture version of the horn with a diameter of 119.8372 mm was measured. There is excellent agreement between the prediction and measurement.

Figure 17 shows the measured and computed difference patterns for the horn at 32.3 GHz. Excellent agreement between the measured and computed patterns is evident. Once again a reduced-aperture

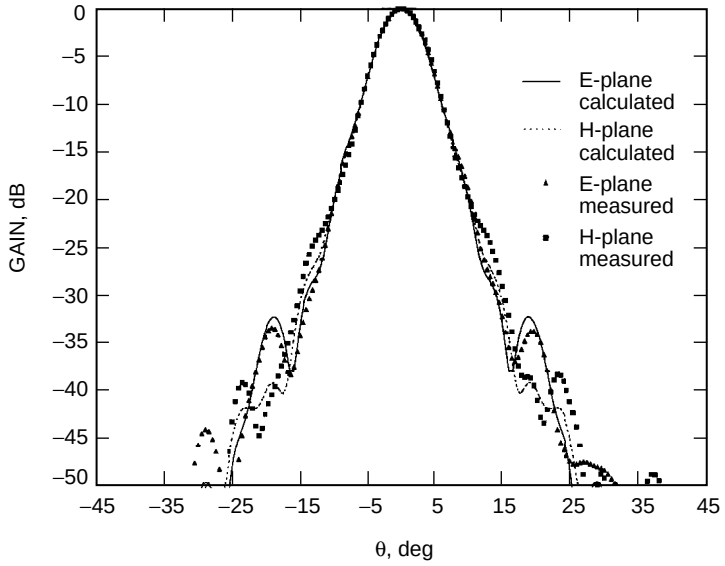

Fig. 16. Measured and computed sum patterns at 32.3 GHz for the reduced horn.

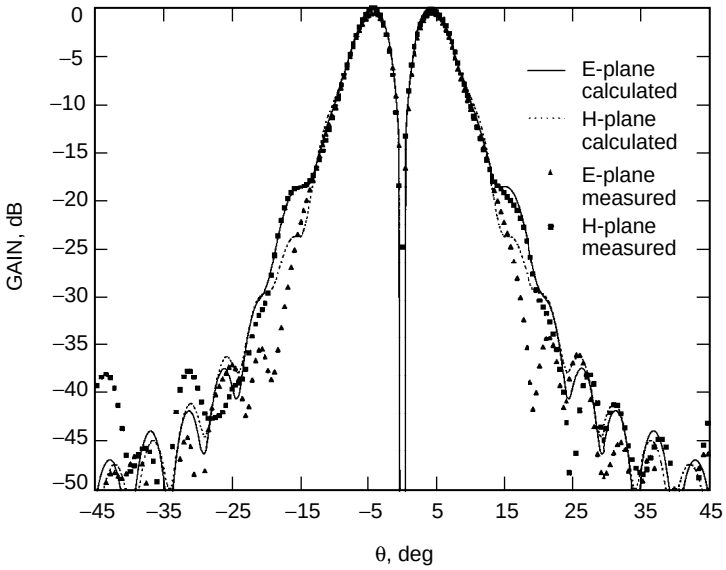

Fig. 17. Measured and computed difference patterns at 32.3 GHz for the reduced horn.

horn was used for this measurement. Figures 18 and 19 show measured and computed patterns for the complete horn at 8.45 and 7.19 GHz. The excellent agreement shown in these figures was also found at other X-band frequencies in the uplink and downlink bands.

Figures 20 through 22 show the predicted sum patterns for the complete horn at 31.8, 32.05, and 32.3 GHz. As was discussed earlier, measurements for this case are not available due to limitations in the near-field range. For the two lower frequencies, a slight dip in the on-axis gain of the feed can be seen. This phenomenon is not uncommon in highly saturated feed horns and has a negligible effect on overall antenna performance. Figures 23 through 25 show the computed difference patterns. In Fig. 23,

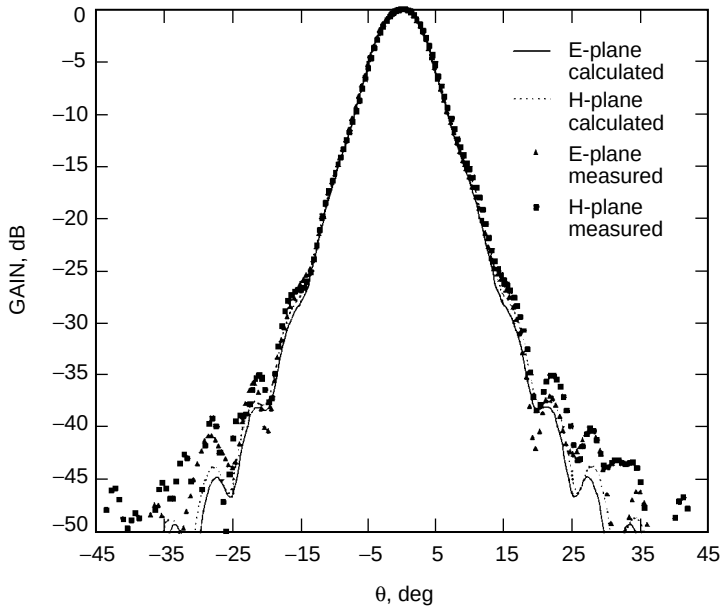

Fig. 18. Measured and computed patterns at 8.45 GHz for the complete horn.

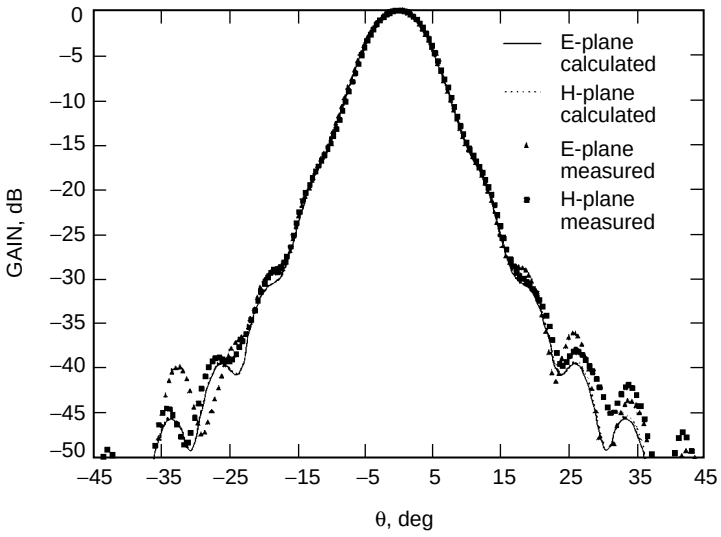

Fig. 19. Measured and computed patterns at 7.19 GHz for the complete horn.

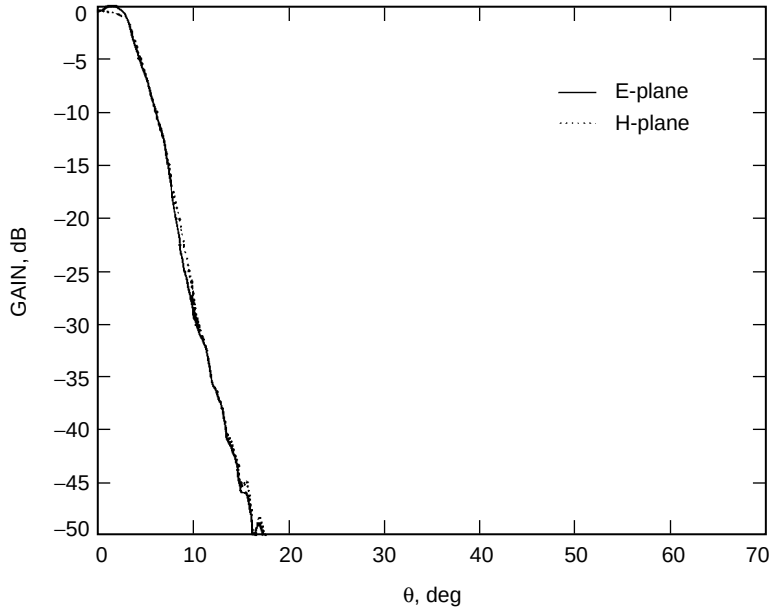

Fig. 20. Computed sum patterns at 31.8 GHz for the complete horn.

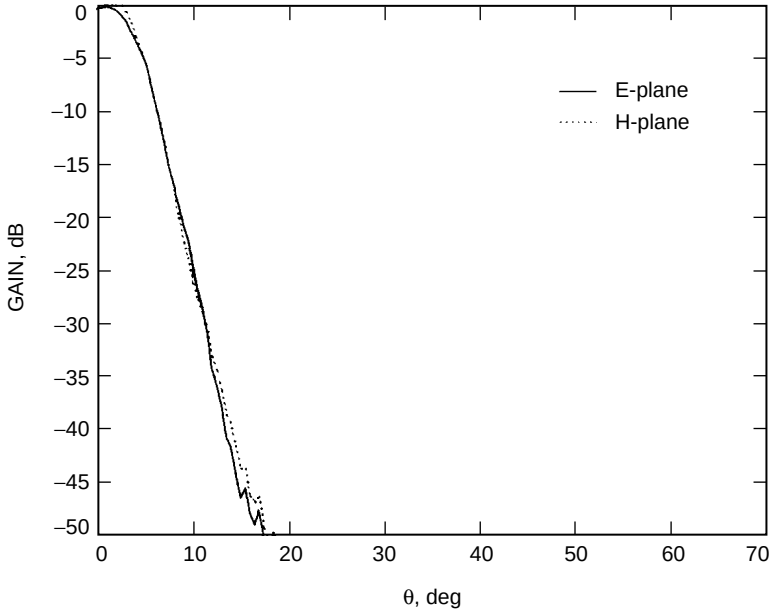

Fig. 21. Computed sum patterns at 32.05 GHz for the complete horn.

the effects of some spurious mode generation are evident at the peak of the difference beam. These effects will be smoothed out after the beam is scattered from the beam-waveguide mirrors, subreflector, and main reflector and have only a minor impact on overall monopulse performance at the low end of the Ka-band. The cause of the spurious mode generation has been traced back to the X-band mode-converter section. Although the depth of the single matching groove was designed to have negligible impact on the Ka-band sum beam, the effect on the difference beam was not considered during the design. Possible solutions to this minor problem are discussed in Section XII.

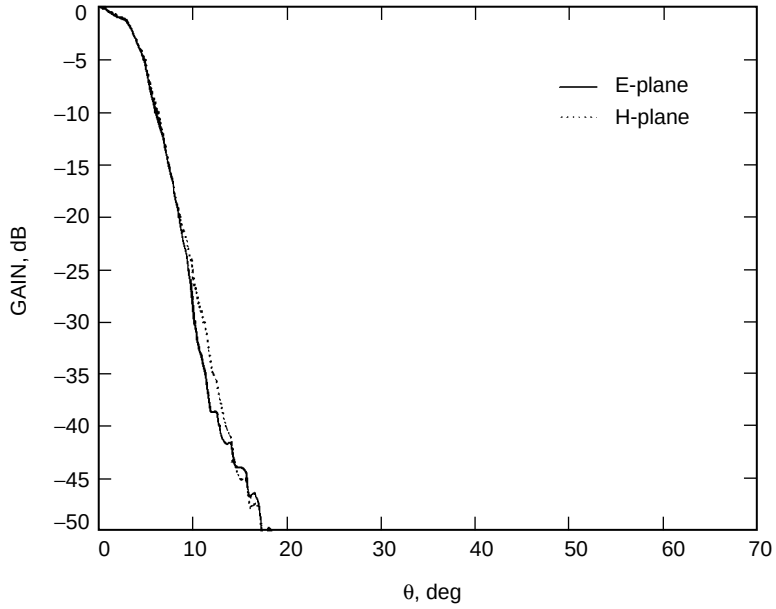

Fig. 22. Computed sum patterns at 32.3 GHz for the complete horn.

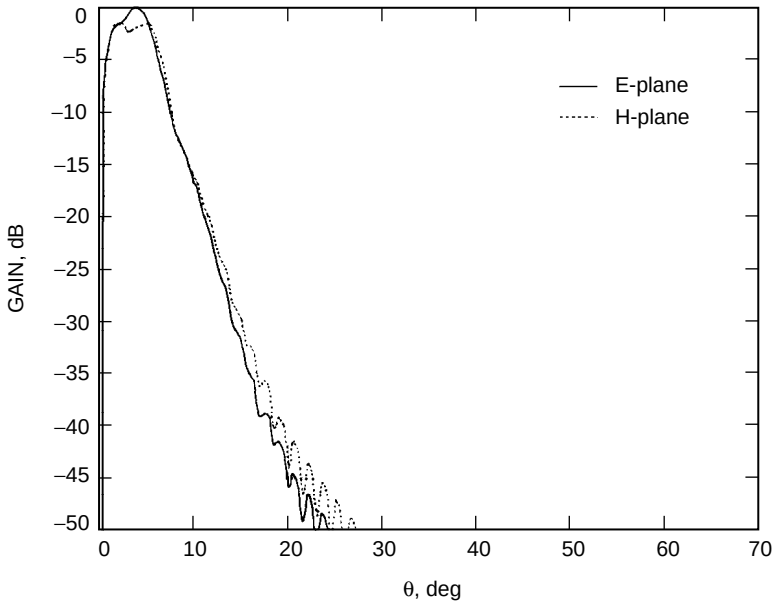

Fig. 23. Computed difference patterns at 31.8 GHz for the complete horn.

XII. Conclusions/Future Work

The overall design for the X-/X-/Ka-band feed has been presented. The key design features of the feed have been described along with some difficulties encountered during its development. A few minor improvements are still desirable. These include the development of a more robust window design and a final iteration of the X-band mode-converter design, considering the effect on the Ka-band difference beam. Windows fabricated using thicker kapton sheets, or more complicated quartz window designs,

could be investigated. The single matching groove could be further optimized or replaced with a pair of grooves to minimize the impact on the Ka-band difference beam. For future versions of the feed, it would be quite valuable to develop a computer model that includes the X-band input junctions. This would allow for exact modeling of the feed at all frequencies, eliminating nearly all the cut and try aspects of the development.

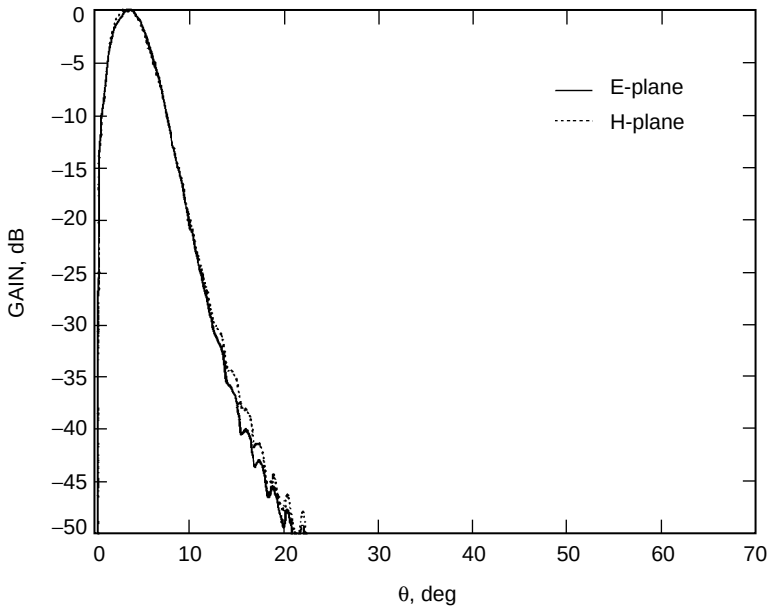

Fig. 24. Computed difference patterns at 32.05 GHz for the complete horn.

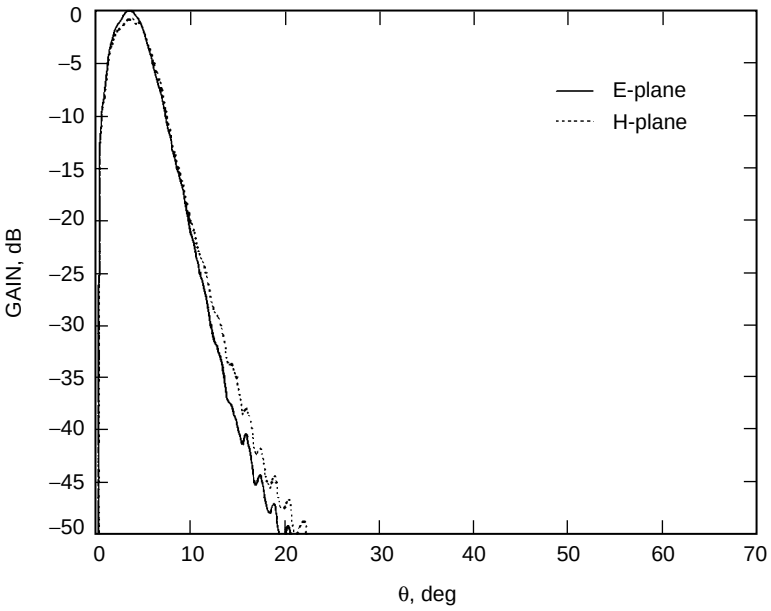

Fig. 25. Computed difference patterns at 32.3 GHz for the full horn.

References

[1] C. D. Edwards, Jr., C. T. Stelzried, L. J. Deutsch, and L. Swanson, "NASA's Deep-Space Telecommunications Road Map," *The Telecommunications and Mission Operations Progress Report 42-136, October–December 1998*, Jet Propulsion Laboratory, Pasadena, California, pp. 1–20, February 15, 1999.
http://tmo.jpl.nasa.gov/tmo/progress_report/42-136/136B.pdf

[2] J. C. Chen, P. H. Stanton, and H. F. Reilly, "Performance of the X-/Ka-/KABLE-Band Dichroic Plate in the DSS-13 Beam Waveguide Antenna," *The Telecommunications and Data Acquisition Progress Report 42-115, July–September 1993*, Jet Propulsion Laboratory, Pasadena, California, pp. 54–64, November 15, 1993.
http://tmo.jpl.nasa.gov/tmo/progress_report/42-115/115e.pdf

[3] Y. H. Choung, K. R. Goudey, and L. G. Bryans, "Theory and Design of a Ku-Band TE_{21}-Mode Coupler," *IEEE Transactions On Microwave Theory and Techniques*, vol. 30, no. 11, pp. 1862–1866, November 1982.

[4] D. J. Hoppe, "Modal Analysis Applied to Circular, Rectangular, and Coaxial Waveguides," *The Telecommunications and Data Acquisition Progress Report 42-95, July–September 1988*, Jet Propulsion Laboratory, Pasadena, California, pp. 89–96, November 15, 1988.
http://tmo.jpl.nasa.gov/tmo/progress_report/42-95/95I.PDF

[5] J. C. Chen, P. H. Stanton, and H. F. Reilly, "X/X/Ka-Band Horn Design," *1996 IEEE International APS Symposium Digest*, Baltimore, Maryland, pp. 2022–2025, July 1996.

[6] W. Veruttipong, J. C. Chen, and D. A. Bathker, "Gaussian Beam and Physical Optics Iteration Technique for Wideband Beam Waveguide Feed Design," *The Telecommunications and Data Acquisition Progress Report 42-105, January–March 1991*, Jet Propulsion Laboratory, Pasadena, California, pp. 128–135, May 15, 1991.
http://tmo.jpl.nasa.gov/tmo/progress_report/42-105/105K.PDF

Appendix

Calibration for Junction Reflection Measurements

As mentioned earlier, for the determination of the feed matching elements, a method to measure the reflection from two diametrically opposed rectangular waveguide ports of the X-/X-/Ka-band feed's uplink and downlink junctions was needed. The reflections from these ports are identical, except 180 deg out of phase, if the part fabrication is precise. These two reflections can be summed in phase by a pair of identical (mirror-image) waveguide arms connected to a matched hybrid tee, as shown in Fig. A-1.

If a calibration can be accomplished at the reference planes, accurate reflection measurements can be made looking into the rectangular waveguide ports of these junctions. A pair of dual-armed combiners is needed to make this calibration (see Fig. A-1). These combiners can be connected together by rotating the 90-deg waveguide elbows as shown in Fig. A-2. The interface planes of these two combiners are the calibration planes where such calibration standards as $\lambda g/4$ lines, shorts, and loads are placed.

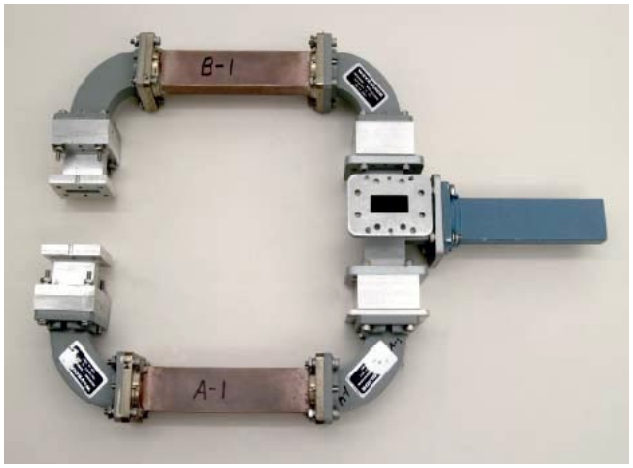

Fig. A-1. The waveguide combiner.

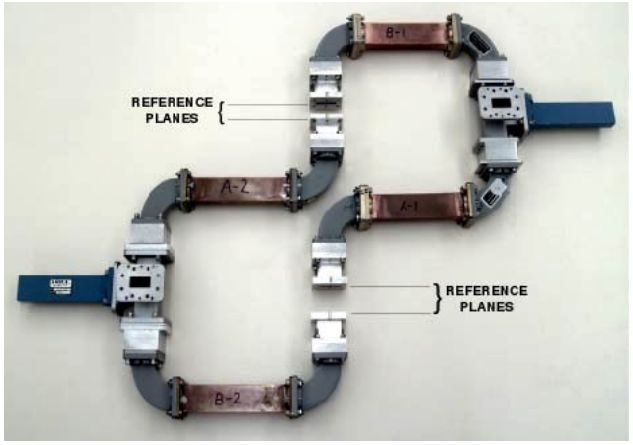

Fig. A-2. A pair of dual-armed waveguide combiners.

Calibration verification standards, in the form of an identical pair of waveguide irises, are inserted at the reference planes, and measurements (S_{11}, S_{21}) of these were compared to the computed values to prove the accuracy of the calibration (Table A-1).

Once calibrated, the 90-deg waveguide elbow is returned to its original position on one of the combiners. This combiner can then be attached to the junction and reflection measurements made.

Because the junction's rectangular waveguide inputs are, in general, nonstandard waveguide sizes, stepped waveguide transforms are included in these combiners. The combiner's phase balance between the two arms is adjusted to be 180 deg $\pm$ 0.5 deg apart.

Table A-1. Calibration verification.

Frequency, GHz	Measured magnitude, phase	Computed magnitude, phase
	S_{11}	
8.4	0.62016, 123.82°	0.61261, 123.57°
8.425	0.61652, 123.48°	0.60815, 123.23°
8.45	0.61106, 123.09°	0.60368, 122.88°
	S_{21}	
8.4	0.77712, −145.99°	0.79038, −146.43°
8.425	0.78073, −146.31°	0.79382, −146.77°
8.45	0.78419, −146.67°	0.79723, −147.12°